Supporting Information

Fluorescent Wood Sponge toward Cr(VI) Selective Detection and Efficient Removal

Dingyuan Zheng[1, 2], Wenrui Yao[1, 2], Ce Sun[1, 2], Xiaojian Chen[1, 2], Jiyuan Zhou[1, 2], Baiwang Wang[1, 2], Haiyan Tan[1, 2], Yanhua Zhang[1, 2, *], Yonggui Wang[1, 2, *]

1. Key Laboratory of Bio-based Material Science & Technology (Northeast Forestry University), Ministry of Education, Harbin 150040, China

2. Engineering Research Center of Advanced Wooden Materials (Northeast Forestry University), Ministry of Education, Harbin 150040, China

*Corresponding author 1. E-mail: zhangyanhua@nefu.edu.cn (Dr. Yanhua Zhang)

*Corresponding author 2. E-mail: wangyg@nefu.edu.cn (Dr. Yonggui Wang)

Contents:

1. Langmuir model and Freundlich model.

2. Pseudo-first-order and pseudo-second-order kinetic models.

3. Figure S1. TEM image (a) and HRTEM image (b, inset: typical single CDs nanoparticles with lattice parameters of 0.21 nm) of CDs; Size distribution of CDs (c); UV-vis and fluorescence spectra of CDs (d); Photos of CDs aqueous under visible light and 365 nm UV light (e); FTIR (f) and XPS spectra (g, h, i) of CDs.

4. Table S1. Chemical components of BW and WS.

5. Figure S2. XPS C 1s spectra of CA/WS (a) and WS (b).

6. Figure S3. Photographs of CA/WS-CDs-x (x=1, 2, 4, and 5) under visible light and 365 nm UV light.

7. Figure S4. SEM images (longitudinal section) of BW (a), WS (b), CA/WS (c), CA/WS-CDs-3 (d) and corresponding EDS mapping images of C, O, and N elements.

8. Figure S5. XPS C 1s spectra (0-40 eV) of CA/WS-CDs-3 sampling at four different locations (a); XPS N 1s (b) and O 1s (c) spectra of CA/WS-CDs-3; O 1s (d) spectra of CA/WS.

9. Figure S6. UV-vis curves of water after CA/WS-CDs (black line) and WS-CDs (red line) immersing for a week.

10. Figure S7. Stress-strain curves of CA/WS-CDs-3 under compression with different maximum strains of 10%, 20%, 30%, and 40% (a); Comparison of the compressible performance for WS (b) and CA/WS-CDs-3 (c).

11. Figure S8. Effect of co-existing anions on the detection performance of Cr(VI) by CA/WS-CDs-3 (adsorbent mass, 50 mg; solution volume, 50 mL; concentration of Cr(VI) solution, 800 mg·L^{-1}; 25 °C, 24 h).

12. Table S2. Parameters of Langmuir model and Freundlich model for Cr(VI) adsorption.

13. Table S3. Parameters of Pseudo-first-order and Pseudo-second-order kinetic models for Cr(VI) adsorption.

14. Figure S9. Effect of co-existing anions on the adsorption capacity of Cr(VI) by

CA/WS-CDs-3 (adsorbent mass, 50 mg; solution volume, 50 mL; concentration of Cr(VI) solution, 800 mg·L^{-1}; 25 °C, 24 h).

1. Langmuir model and Freundlich model

Langmuir model and Freundlich model are expressed as follows:

$$C_e / q_e = C_e / q_m + 1 / (bq_m) \tag{1}$$

$$log q_e = log k + (1 / n) log C_e \tag{2}$$

Where C_e (mg·L^{-1}) represents the residual concentration after reaching equilibrium; q_e (mg·g^{-1}) stands for the equilibrium adsorbing capacity; q_m (mg·g^{-1}) stands for the maximum adsorbing capacity; b (L·mg^{-1}) represents the Langmuir constant, while k ((mg·g^{-1}) (L·mg^{-1})$^{1/n}$) and n stand for Freundlich constants.

2. Pseudo-first-order and pseudo-second-order kinetic models

Pseudo-first-order and pseudo-second-order kinetic models are expressed as follows:

$$ln(q_e - q_t) = ln q_e - k_1 t \tag{3}$$

$$t / q_t = 1 / (k_2 q_e^2) + t / q_e \tag{4}$$

Where q_e (mg·g^{-1}) stands for the equilibrium adsorbing capacity; q_t (mg·g^{-1}) stands for the adsorbing quantity at time t (min); k_1 (min^{-1}) and k_2 (g·mg^{-1}·min^{-1}) are rate constants for stand for Pseudo-first-order and pseudo-second-order kinetic models, respectively.
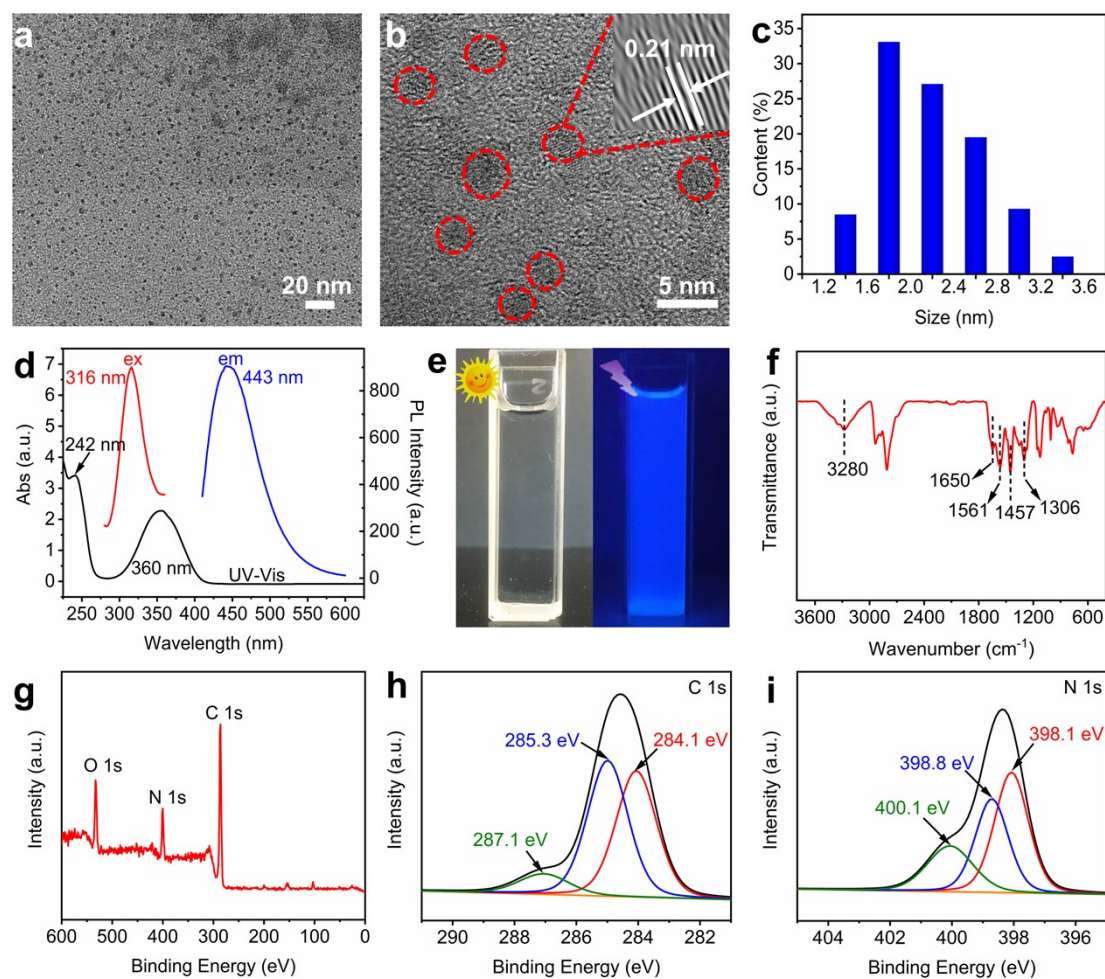
Figure S1. TEM image (a) and HRTEM image (b, inset: typical single CDs nanoparticles with lattice parameters of 0.21 nm) of CDs; Size distribution of CDs (c); UV-vis and fluorescence spectra of CDs (d); Photos of CDs aqueous under visible light and 365 nm UV light (e); FTIR (f) and XPS spectra (g, h, i) of CDs.

CDs were synthesized using CA as a carbon source and PEI as a passivation agent via the hydrothermal process. The obtained CDs show spherical morphology (**Figure S1a, b**), with a diameter range from 1.2 nm to 3.6 nm (**Figure S1c**). High-resolution TEM image for CDs with higher solution reveals the typical graphite facet (100) with a lattice spacing of 0.21 nm (**Figure S1b**).[1,2] In theory, CDs have fluorescent properties, which could be visually confirmed with the intense blue emission under 365 nm UV light (**Figure S1e**). To further clarify CDs' fluorescence characteristics, UV-vis and fluorescence spectra tests were

performed (**Figure S1d**). The UV-vis spectrum shows two clear absorption bands at 242 (π-π^*, transition of the aromatic ring) and 360 nm (n-π^*, the transition of C=O), which was consistent with previous reports.[1,2] Additionally, the maximum excitation and emission wavelength for prepared CDs aqueous are fixed at 316 nm and 443 nm, respectively.

The chemical properties are the decisive factors that affect the loading of CDs on WS. Hence, FTIR spectroscopy and XPS analysis were used to characterize the surface chemistry of CDs. As shown in **Figure S1f**, the broad-band at around 3280 cm^{-1} represents the existence of -OH and -NH.[1,3] Peaks at 1561, 1457, and 1306 cm^{-1} are attributed to N-H, CH_2, and C-N, respectively.[1] The peak at 1650 cm^{-1}, which is attributed to -CONH-, demonstrates that PEI was successfully grafted onto the surface of CDs.[1] In addition, the results of the XPS spectra further confirmed the presence of the amino groups in CDs (**Figure S1g**). As shown in **Figure S1h**, the high-resolution XPS spectra of C 1s are deconvolved into three peaks unit moieties, namely, C=C/C-C bond at 284.1 eV, C-OH/C-O-C with binding energy at 285.3 eV and -CN- at 287.1 eV.[1] The high-resolution XPS spectrum of N1s (**Figure S1i**) exhibits three peaks at 398.1, 398.8, and 400.1 eV, which correspond to pyridinic, pyrrolic, and graphitic N/N-H, respectively.[2] The presence of amino groups will undoubtedly facilitate the loading of CDs on the CA/WS.
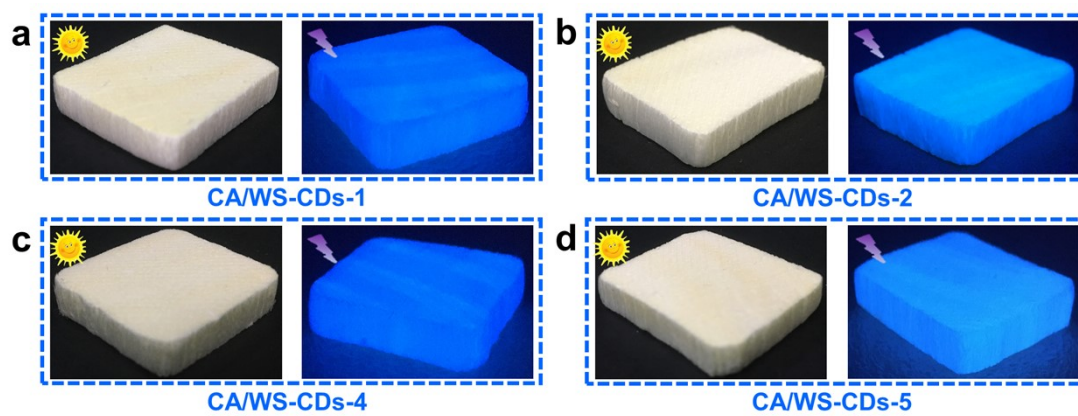
Table S1 The chemical components of samples

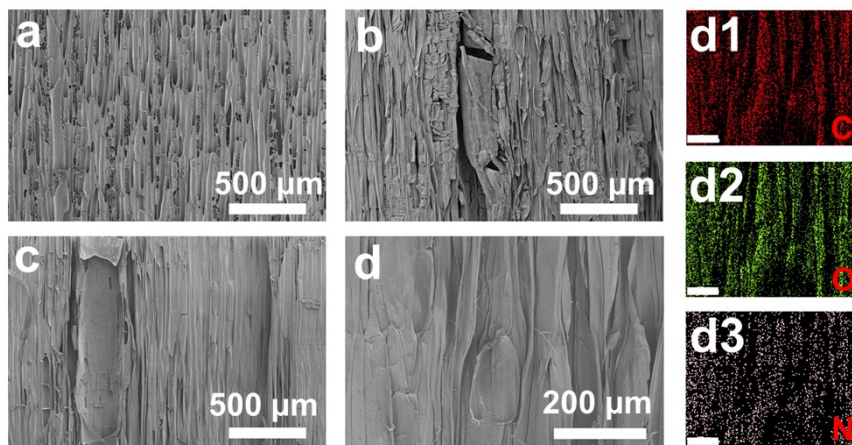| Samples	Organic extracts (%)	Cellulose (%)	Lignin (%)	Hemicellulose (%)
BW	2.37	40.32	16.74	23.26
WS	0.66	72.13	0.73	17.51
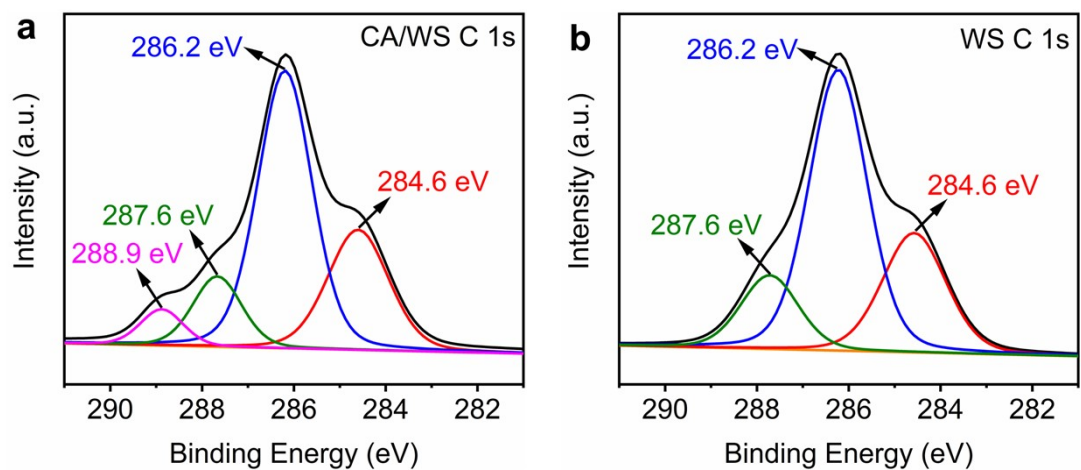
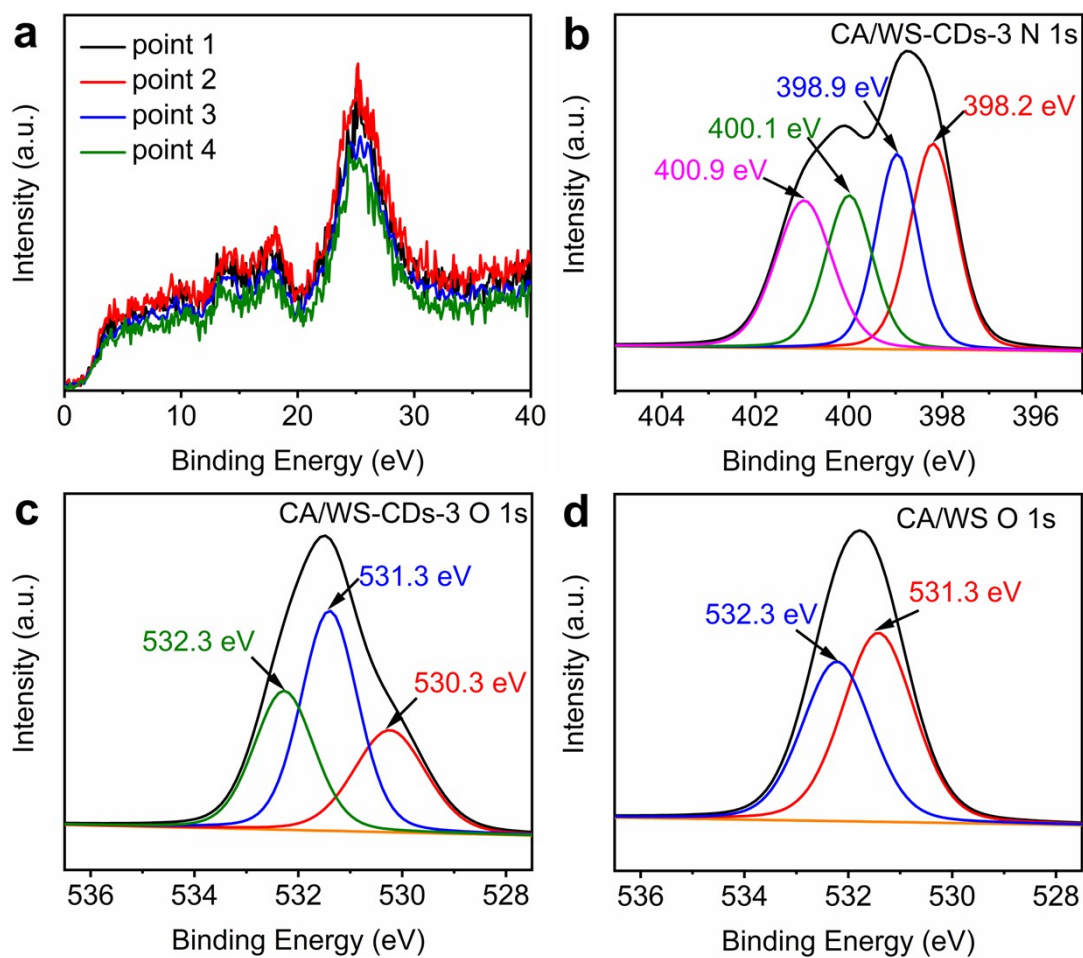**Figure S2.** XPS C 1s spectra of CA/WS (a) and WS (b).

Figure S3. Photographs of CA/WS-CDs-x (x=1, 2, 4, and 5) under visible light and 365 nm UV light.

Figure S4. SEM images (longitudinal section) of BW (a), WS (b), CA/WS (c), CA/WS-CDs-3 (d) and corresponding EDS mapping images of C, O, and N elements.

Figure S5. XPS C 1s spectra (0-40 eV) of CA/WS-CDs-3 sampling at four different locations (a); XPS N 1s (b) and O 1s (c) spectra of CA/WS-CDs-3; O 1s (d) spectra of CA/WS.
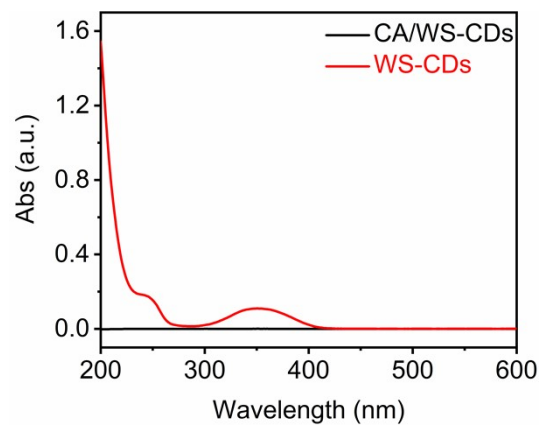
Figure S6. UV-vis curves of water after CA/WS-CDs (black line) and WS-CDs (red line) immersing for a week.
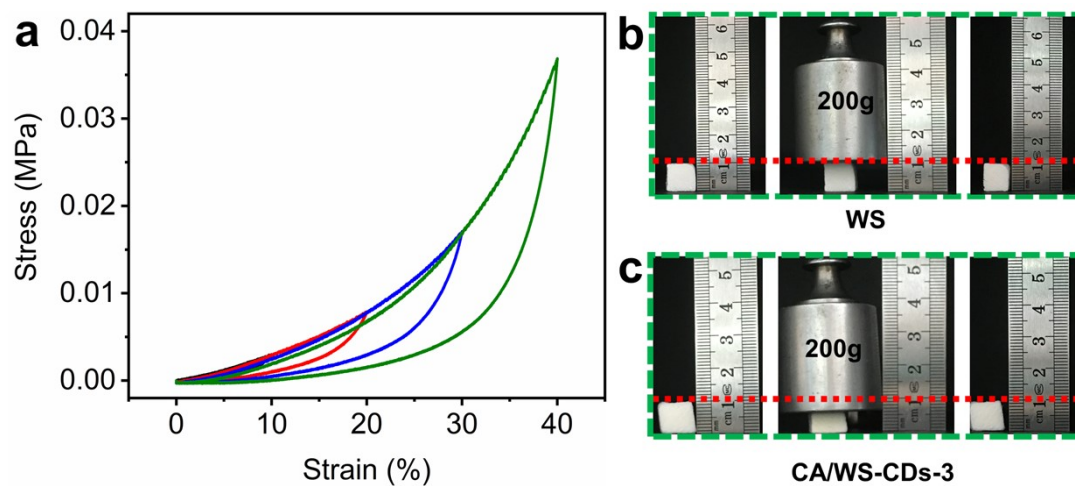
Figure S7. Stress-strain curves of the wood sponge under compression with different maximum strains of 10%, 20%, 30%, and 40% of CA/WS-CDs-3 (a); Comparison of the compressible performance for WS (b) and CA/WS-CDs-3 (c).
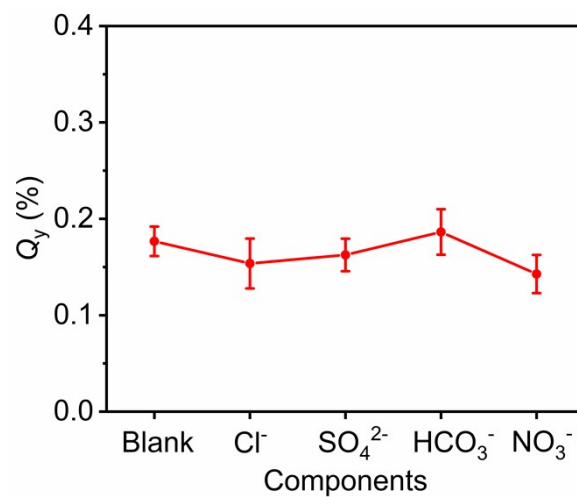
Figure S8. Effect of co-existing anions on the detection performance of Cr(VI) by CA/WS-CDs-3 (adsorbent mass, 50 mg; solution volume, 50 mL; concentration of Cr(VI) solution, 800 mg·L^{-1}; 25 °C, 24 h).

Table S2 Parameters of Langmuir model and Freundlich model for Cr(VI) adsorption

| Sample	Langmuir model parameters			Freundlich model parameters		
	q_m(mg·g^{-1})	b(L·mg^{-1})	R^2	n	k((mg·g^{-1}) (L·mg^{-1})$^{1/n}$)	R^2
CA/WS-CDs-3	450.5	0.011	0.993	1.84	17.52	0.948

Table S3 Parameters of Pseudo-first-order and Pseudo-second-order kinetic models for Cr(VI) adsorption

| Sample	Pseudo-first-order model			Pseudo-second-order model		
	k_1(min^{-1})	q_e(mg·g^{-1})	R^2	k_2(g·mg^{-1}·min^{-1})	q_e(mg·g^{-1})	R^2
CA/WS-CDs-3	0.001	348.1	0.943	0.0001	478.5	0.994
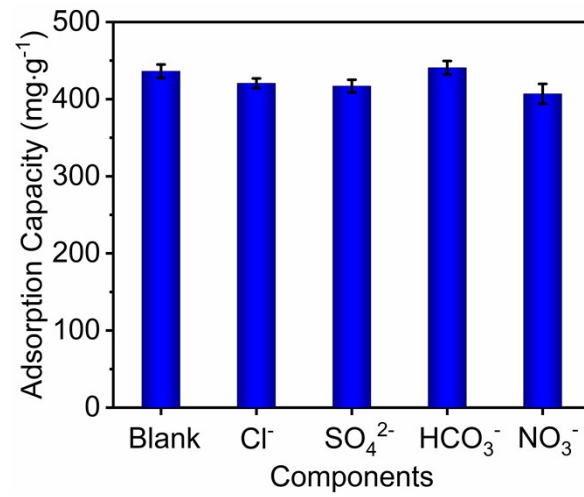
Figure S9. Effect of co-existing anions on the adsorption capacity of Cr(VI) by CA/WS-CDs-3 (adsorbent mass, 50 mg; solution volume, 50 mL; concentration of Cr(VI) solution, 800 $mg \cdot L^{-1}$; 25 °C, 24 h).
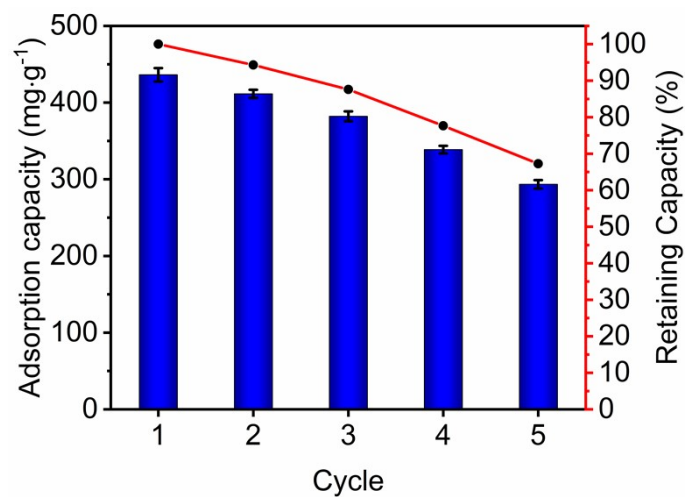
Figure S10. Regeneration performance of CA/WS-CDs-3 (adsorbent mass, 50 mg; solution volume, 50 mL; concentration of Cr(VI) solution, 800 mg·L^{-1}; 25 °C, 24 h).
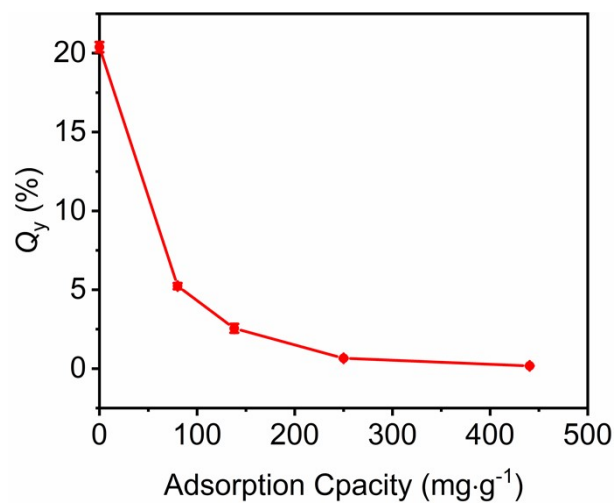
Figure S11. The relation between quantum yield (Q_y, %) of CA/WS-CDs-3 and adsorption capacity after immersed in diverse initial concentrations for 24 h.
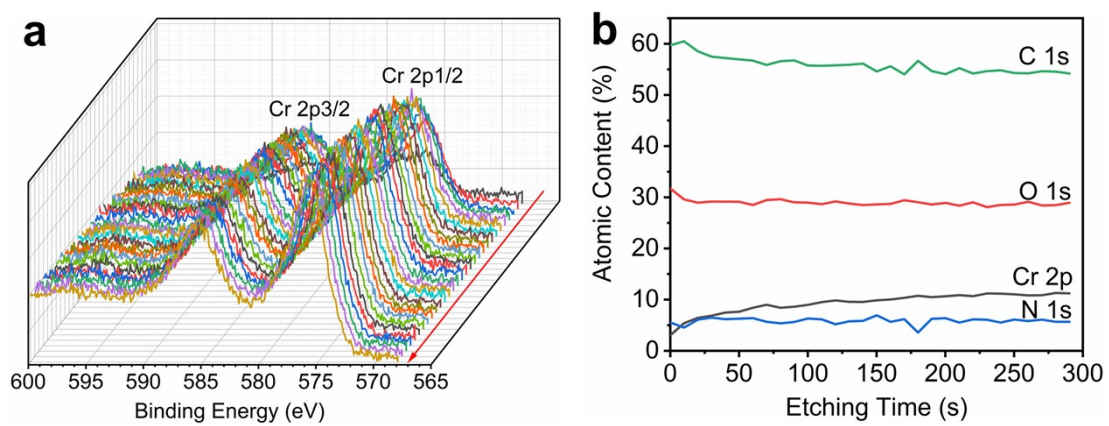
Figure S12. XPS spectra of 30 layers of CA/WS-CDs-3 etching with Ar atom after adsorption (a) and atomic content of different atoms within etching process (b).
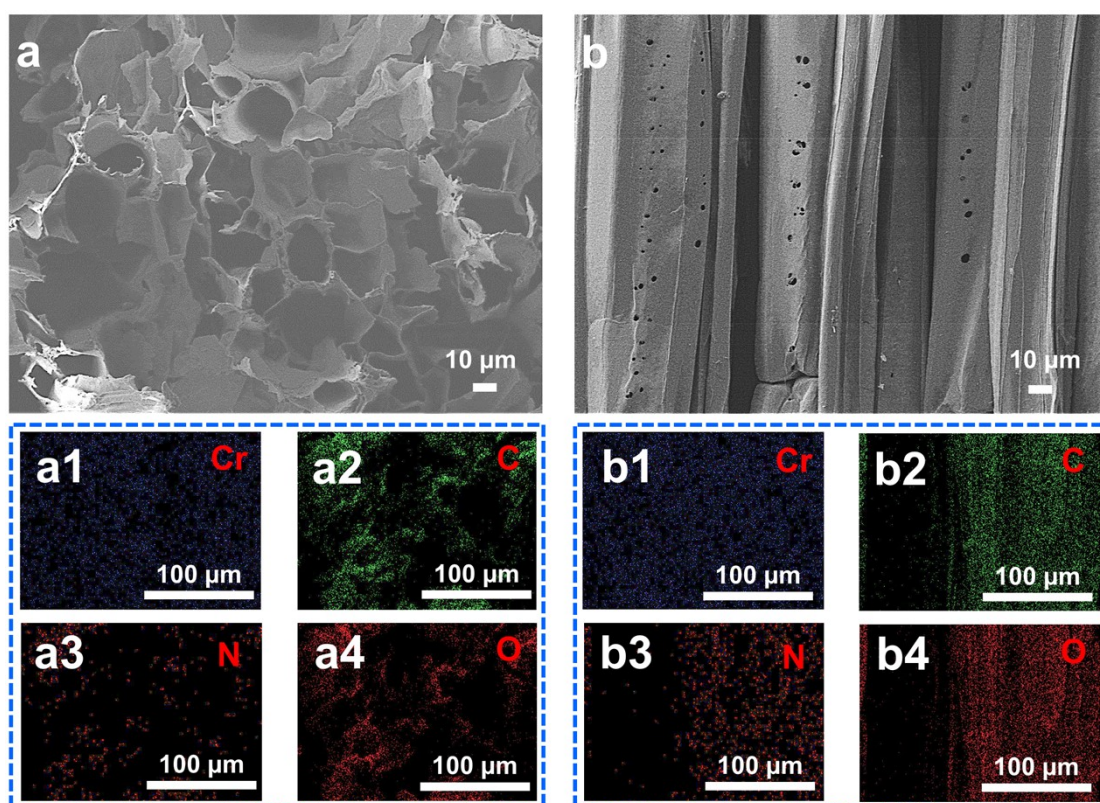
Figure S13. SEM images (internal cross section (a) and internal longitudinal section (b)) and corresponding EDS mapping images of CW/WS-CDs-3 after adsorption.

Table S4 The ratios of Cr 2p components of CA/WS-CDs-3 before and after Cr(VI) adsorption

Samples	Cr 2p components (at. %)			
	Cr-N-Cr (Cr(VI))	Cr-N-Cr (Cr(III))	N-Cr (Cr(VI))	N-Cr (Cr(III))
1#	-	-	-	-
2#	36.86	32.42	7.10	23.62

Note: 1# and 2# represent CA/WS-CDs-3 before and after Cr(VI) adsorption, respectively.

Table S5 The at. % of C, O, N, Cr and ratios of O 1s components of CA/WS-CDs-3 before and after Cr(VI) adsorption

Samples	Elements (at. %)				O1s components (at. %)			
	C 1s	O1s	N 1s	Cr 2p	-CONH-	C-OH	Cr-O	C-O-C
1#	61.47	30	8.53	-	25.57	44.94	-	29.49
2#	59.59	33.58	4.69	2.15	10.71	22.83	37.49	28.97

Note: 1# and 2# represent CA/WS-CDs-3 before and after Cr(VI) adsorption, respectively.
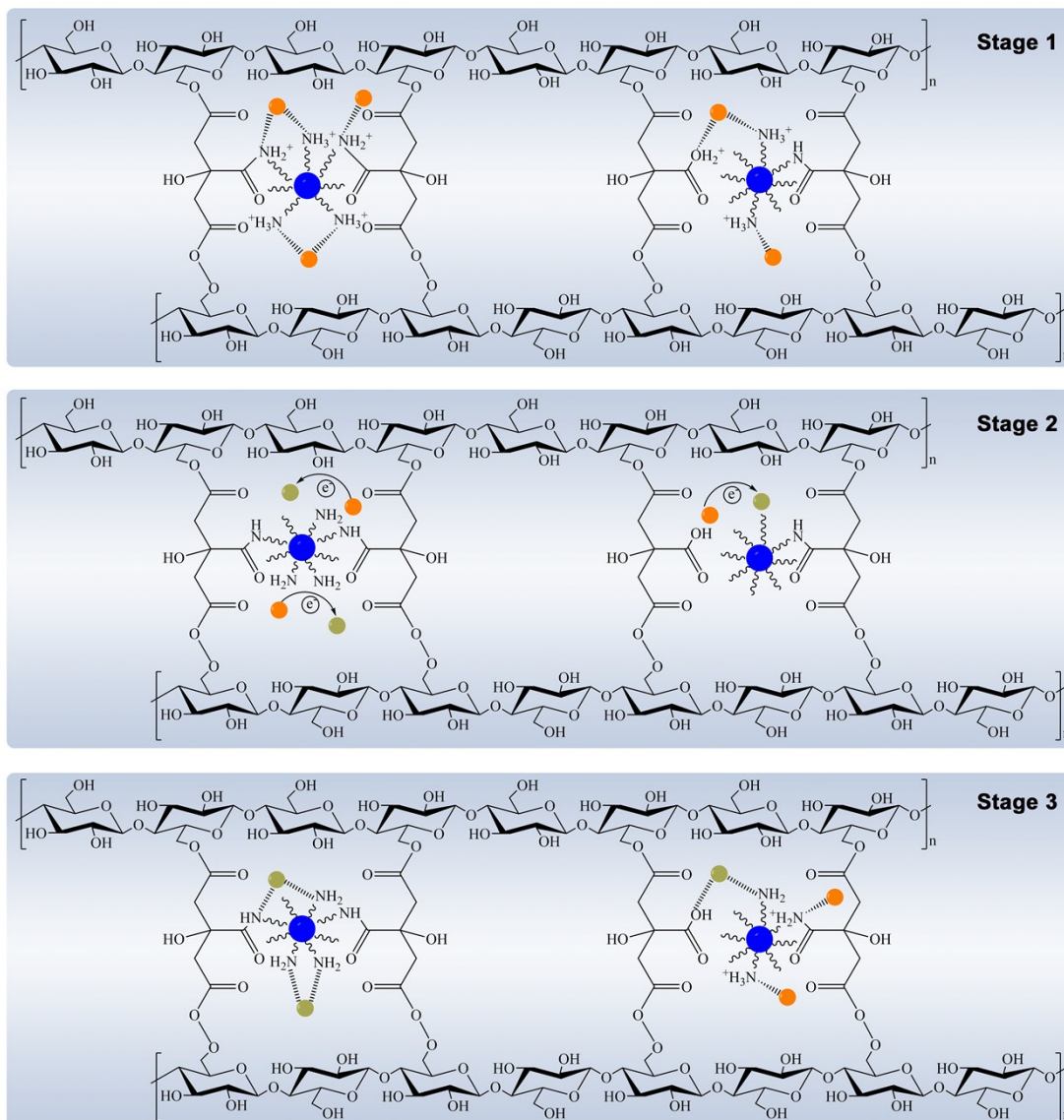
Figure S14. Possible adsorption process of Cr(VI) on to CA/WS-CDs-3.

References

[1] B. Wu, G. Zhu, A. Dufresne and N. Lin, Fluorescent aerogels based on chemical crosslinking between nanocellulose and carbon dots for optical sensor, *ACS Appl. Mater. Inter.*, 2019, 11, 16048-16058.

[2] M. Zheng, S. Liu, J. Li, D. Qu, H. Zhao, X. Guan, X. Hu, Z. Xie, X. Jing and Z. Sun, Integrating oxaliplatin with highly luminescent carbon dots: an unprecedented theranostic agent for personalized medicine, *Adv. Mater.*, 2014, 26, 3554-3560.

[3] X. Guo, D. Xu, H. Yuan, Q. Luo, S. Tang, L. Liu and Y. Wu, A novel fluorescent nanocellulosic hydrogel based on carbon dots for efficient adsorption and sensitive sensing in heavy metals, *J. Mater. Chem. A*, 2019, 7, 27081-27088.